Brain Tumor Pathology (2019) 36:103–111
https://doi.org/10.1007/s10014-019-00344-z

ORIGINAL ARTICLE

Clinicopathological characteristics of circumscribed high-grade astrocytomas with an unusual combination of *BRAF* V600E, *ATRX*, and *CDKN2A/B* alternations

Chiaki Murakami[1] · Yuka Yoshida[1] · Tatsuya Yamazaki[1] · Ayako Yamazaki[1] · Satoshi Nakata[2] · Yohei Hokama[3] · Shogo Ishiuchi[3] · Jiro Akimoto[4] · Yukiko Shishido-Hara[5] · Yuhei Yoshimoto[2] · Nozomi Matsumura[1] · Sumihito Nobusawa[1] · Hayato Ikota[1] · Hideaki Yokoo[1]

Received: 12 March 2019 / Accepted: 27 March 2019 / Published online: 10 April 2019

Abstract

We report four cases of high-grade astrocytoma with a *BRAF* V600E mutation, *ATRX* inactivation, and *CDKN2A/B* homozygous deletion. Children to young adults aged 3–46 presented with a well demarcated contrast-enhancing mass in the supratentorial area. Pathological examination revealed packed growth of short spindle to round polygonal cells including some pleomorphic cells. The tumors had less ability to infiltrate into the adjacent brain parenchyma and presented a circumscribed growth pattern. Mitosis was readily found, accompanied by focal necrosis and/or microvascular proliferation. Tumors were histologically similar in part to pleomorphic xanthoastrocytoma (PXA) or anaplastic PXA, but did not fit criteria for either neoplasm. A *BRAF* V600E mutation and homozygous deletion of *CDKN2A/B* were observed, which is similar to the genetic features of PXA or epithelioid glioblastoma, but the additional loss of ATRX nuclear immunoreactivity and absence of *TERT* promoter mutation were unusual findings, indicating a novel genetic profile. Despite their malignant histological features, all patients had a favorable clinical course and remained alive for 6 months to 28 years under standard medical treatment for malignant glioma. In summary, high grade astrocytomas with *BRAF* V600E, *ATRX*, and *CDKN2A/B* alternations had unique clinicopathological features and may be a novel subset of high grade glioma.

Keywords High-grade astrocytoma · Circumscribed astrocytoma · *BRAF* V600E · *ATRX* · *CDKN2A/B*

Introduction

Astrocytic tumors can be separated by their growth pattern, either diffuse or localized. Diffuse astrocytic tumors include diffuse astrocytoma, anaplastic astrocytoma, and glioblastoma. These tumors are mainly located in the supratentorial white matter and are characterized by diffuse infiltration. Localized astrocytomas, such as pilocytic astrocytoma and pleomorphic xanthoastrocytoma (PXA), have less ability to infiltrate into the adjacent brain parenchyma and tend to show a solid growth pattern in the subarachnoid space. Diffuse astrocytic tumors have an *IDH1/2* mutation, frequent inactivation of *ATRX*, and mutation of *TP53*, whereas localized astrocytomas tend to have mutations in the MAPK pathway such as *BRAF*.

PXA with increased mitotic activity (≧ 5 mitoses per 10 high-powered fields) was recognized by the WHO classification criteria in 2016 as anaplastic PXA (A-PXA). A-PXAs have typical histological features of PXA, such as

Electronic supplementary material The online version of this article (https://doi.org/10.1007/s10014-019-00344-z) contains supplementary material, which is available to authorized users.

✉ Chiaki Murakami
m15702002@gunma-u.ac.jp

[1] Department of Human Pathology, Gunma University Graduate School of Medicine, 3-39-22, Showa, Maebashi 371-8511, Gunma, Japan

[2] Department of Neurosurgery, Gunma University Graduate School of Medicine, Maebashi, Japan

[3] Department of Neurosurgery, University of the Ryukyus Graduate School of Medicine, Okinawa, Japan

[4] Department of Neurosurgery, Tokyo Medical University, Tokyo, Japan

[5] Department of Pathology, Tokyo Medical University, Tokyo, Japan

proliferation of spindle-shaped cells with intermingled pleomorphic cells or xanthomatous cells, abundant eosinophilic granular bodies, and rich pericellular reticulin fibers [1]. PXA and A-PXA commonly have a *BRAF* V600E mutation and a homozygous deletion of *CDKN2A/B*. Moreover, *TERT* promoter mutations occasionally occur in PXA (20.5% in PXA, 23–47% in A-PXA) [2, 3], but *ATRX* inactivation is rare.

Here, we report four cases of high grade astrocytomas with an unusual combination of a *BRAF* V600E mutation, *CDKN2A/B* homozygous deletion, and *ATRX* inactivation. We discuss the histopathological differences between these tumors and other astrocytic tumors including PXA.

Materials and methods

Tumor samples

Four cases of high-grade astrocytoma, which had *ATRX* inactivation and *BRAF V600E* mutation by immunohistochemistry and DNA sequence, were recruited. Two cases were from the pathology archives of the Department of Pathology, Gunma University Hospital. One was reported previously (Case 2) [4]. The other two cases were from the pathology archives of the Tokyo Medical University Hospital and the University of Ryukyus Graduate School of Medicine. This research was approved by the ethics committee of Gunma University.

Clinical data

Clinical data and images were obtained from the charts and clinicians of each hospital.

Conventional histological analysis

Tissue specimens were fixed in 10% formalin and embedded in paraffin. Three-micrometer-thick tissue sections were stained with hematoxylin and eosin. For immunohistochemistry, the following primary antibodies were used: Glial fibrillary acidic protein (GFAP; polyclonal, 1:5,000: our own), Olig2 (polyclonal, 1:5000; IBL, Takasaki, Japan), S-100 protein (polyclonal, 1:10,000; our own), Nestin (monoclonal, 1:200; Merck Millipore, Billerica, MA, USA), CD34 (monoclonal, 1:200; Nichirei, Tokyo, Japan), p53 protein (monoclonal, 1:50; Leica Microsystems, Wetzlar, Germany), ATRX (polyclonal, 1:500; Sigma, St. Louis, MO, USA), BRAF V600E epitope (monoclonal, 1:50; Spring Bioscience, Pleasanton, CA, USA), Isocitrate dehydrogenase 1 (IDH1)-R132H (monoclonal, 1:50; Dianova, Hamburg, Germany), and Ki-67 (MIB-1; monoclonal, 1:100; Dako). For GFAP, S-100P, Nestin, Olig2, EMA, CD34, ATRX, and BRAF V600E, the intensity of the staining was graded as negative, weak, moderate or strong, and the extent was scored as follows: (−) totally negative (1+) < 10% of tumor cells were positive (2+) 10–50% of tumor cells were positive, and (3+) more than 50% of tumor cells were positive. The Ki-67 labeling index (LI) was measured by Gunma-LI (Version 017; Japan Brain Tumor Reference Center, Gunma, Japan; available at https://www.jbtrc.com/05_mib04.php).

Direct DNA sequencing for *BRAF, IDH1/2, TP53,* and *TERT* promoter mutations

DNA was extracted from paraffin sections as previously described [5] and was amplified and sequenced using the primers described previously [6–9] (Supplementary material, Table 1). PCR products were sequenced on a 3130xl Genetic Analyser (Applied Biosystems, Foster City, CA, USA) with the Big Dye Terminator v.1.1 Cycle Sequencing kit (Applied Biosystems) following standard procedures.

Multiplex ligation-dependent probe amplification (MLPA) analysis

Copy number changes in the *CDKN2A/B* genes and chromosomes 1 and 19 were analyzed by multiplex ligation-dependent probe amplification (MLPA) as described previously [10].

Results

Clinical findings

The clinical features of each case are shown in Table 1. There were three females and one male. Their age of onset ranged from 3 to 41 years. The symptoms at presentation were headache, epilepsy, impaired consciousness, and facial spasm. Imaging features revealed similar findings in all cases. The tumors were located within the cerebral hemispheres; cases 1, 2, and 4 in the temporal lobe, and case 3 in the frontal lobe. The examination of gadolinium-enhanced T1-weighted magnetic resonance imaging (MRI) revealed well demarcated, nodular, contrast-enhancing lesions (Fig. 1a, e, g, j). In the recurrent tumor of case 2, heterogeneous enhancement was observed (Fig. 1e), whereas other cases were uniformly enhanced (Fig. 1a, g, j). Mild to-moderate edema surrounding the tumor was observed by T2-weighted MRI (Fig. 1b, f, h, k). No calcification was detected by computed tomography (Fig. 1c, i, l). Gross total resection and adjuvant chemoradiotherapy was performed in all patients. The follow-up period from the first operation ranged from 6 months to 28 years. Case 1 and 2 recurred

Table 1 Clinical features

Case	Age	Sex	Location	Images	Symptoms	Treatment	Prognosis
1	46	F	Left temporal lobe	Well demarcated mass on MR (CE) with focal edema; 6×4 cm	Epilepsy (41y.o.−), worsening headache (45y.o. −)	GTR, TMR + radiochemotherapy	Recurrence (50y.o.), additional TMZ + bevacizumab, alive for 7 years after first surgery
2	3	M	Right temporal lobe	Hemorrhagic mass with heterogeneous enhancement (only CT scan)	Impaired consciousness	GTR, radiotherapy (33Gy) + platinum-based chemotherapy	Recurrence (26y.o.)
2 (rec)	26		Right temporal lobe	Heterogeneously enhanced mass on MR (CE) with focal surrounding edema; 7×5 cm	Worsening headache	Resection TMZ + bevacizumab	Alive for 5 years after second surgery
3	35	F	Right frontal lobe	Well demarcated mass on MR (CE) with focal edema	Left facial spasm, headache	GTR + radiotherapy + TMZ	Alive without recurrence for a year
4	32	F	Left temporal lobe	Well demarcated mass on MR (CE) with focal edema	Headache	GTR + radiotherapy + TMZ	Alive without recurrence for 6 months

(rec) recurrence, *M* male, *F* female, *y.o.* years old, *MR (CE)* magnetic resonance with contrast enhancement, *GTR* gross total resection, *TMZ* temozolomide

23 years and 4 years after surgery, respectively, and all patients remained alive.

Histological findings

A summary of the histological features is presented in Table 2. The ratio of cellular elements was assayed by visual estimation. All tumors had a solid growth pattern, with case 1, 2, and 3 showing a slight degree of infiltration to the adjacent brain parenchyma (Fig. 2a). In case 1, tumor extension along the parenchymal vessels and subpial accumulation of tumor cells was found (Fig. 2b). Medium-sized muscular arteries were entrapped in all cases, which suggests exophytic tumor growth into the subpial space.

All tumors were mainly composed of short spindle cells with round-to-oval nuclei and thick processes arranged in a fascicular pattern (Fig. 2c, d). Tumor cells with round cytoplasm and eccentric nuclei resembling epithelioid cells were occasionally seen (Fig. 2e). Large mono- or multi-nucleated pleomorphic cells were focally observed (Fig. 2f). A xanthomatous change was seen in case 2, but not conspicuous. Unlike conventional PXAs, eosinophilic granular bodies were found only in case 4 (Fig. 2g), and not apparent in the other cases. Reticulin fibers surrounding tumor cells were not observed by silver staining (Fig. 2h). Thick hyalinization of the vessel wall was found in case 2. Invasion of tumor cells into the vascular wall was seen in cases 3 and 4. Concentric fibrosis around blood vessels was observed in case 4. An increase of small vessels was observed in all cases, and a small number of microvascular proliferations was detected in cases 1, 4, and the recurrent tumor of case 2. Relatively high levels of mitotic activity were seen with brisk mitotic figures ranging from 4 to 20 per 10 high-powered fields. Palisading necrosis was identified in cases 1 and 2 (Fig. 2i).

Immunohistochemistry

The immunohistochemical findings are summarized in Table 2. All tumors were diffusely positive for S-100 protein, Olig2, and Nestin (Fig. 3a, b). Spindle-shaped cells were diffusely-to-sparsely positive for GFAP (Fig. 3c). CD34 immunoreactivity was not detected in any tumors. Loss of ATRX nuclear expression (Fig. 3d) and BRAF V600E immunoreactivity and were observed in all cases (Fig. 3e). The Ki-67 labeling index ranged from 6.1 to 20.1% (Gunma-LI) (Fig. 3f).

Genetic findings

A *BRAF V600E* mutation (Fig. 4a) and *CDKN2A/B* homozygous deletion (Fig. 4b) were detected in all cases by direct DNA sequencing or MLPA analysis. The *TERT* promoter and *IDH1/2* were intact. Direct sequencing of *TP53* revealed an R248Q mutation in case 3 (data not shown).

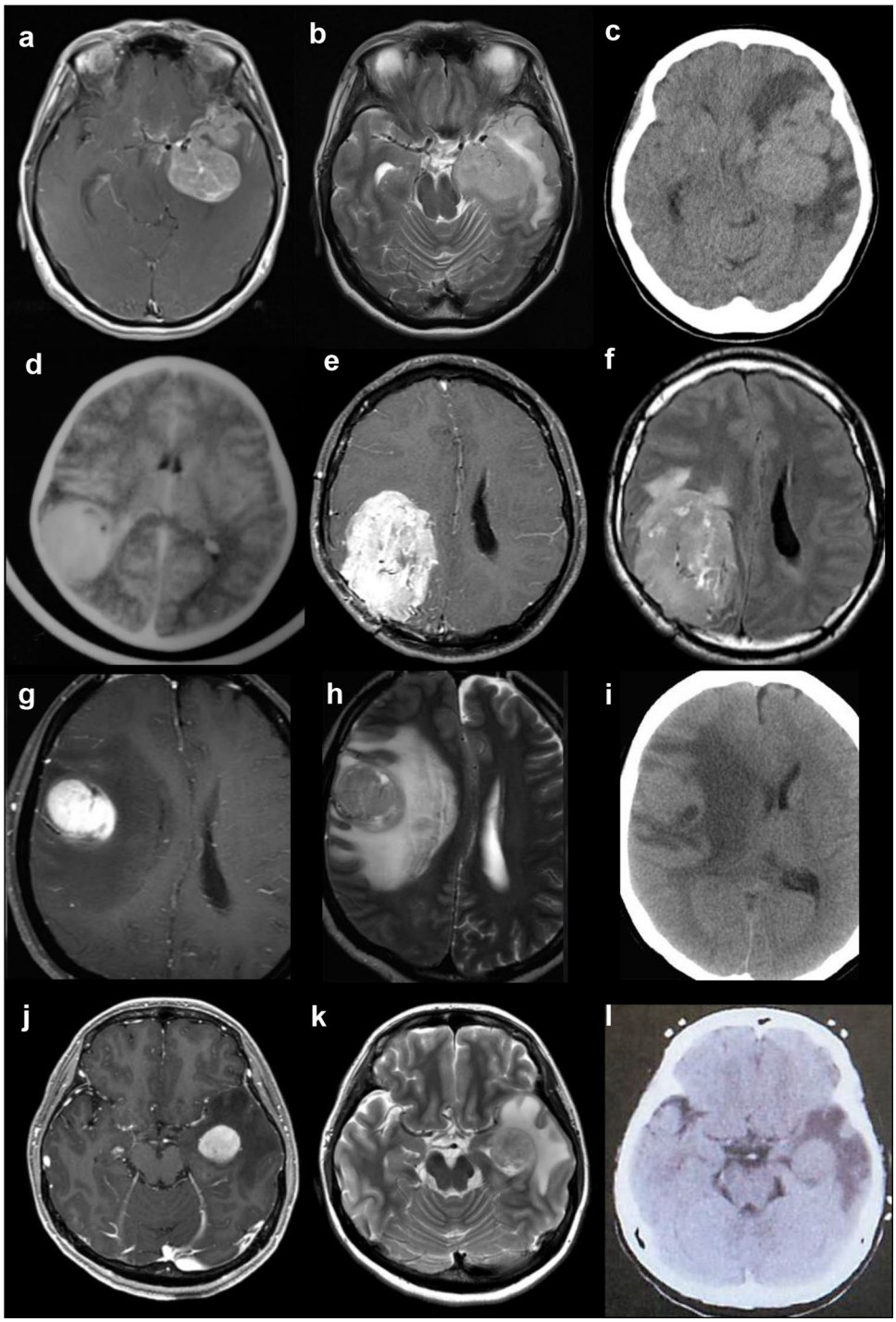

Fig. 1 Radiological images of all four cases. Case 1 (**a**–**c**). **a** Gadolinium-enhanced T1-weighted image (Gd-T1WI) shows a well demarcated mass by a homogeneous enhancement. **b** A Fluid attenuated inversion recovery (FLAIR) image shows peritumoral edema. **c** Calcification was not detected by computed tomography (CT). Case 2 (**d**–**f**). **d** Contrast-enhanced CT image of the initial onset when the patient was 3 years old. A circumscribed mass with hemorrhage was located within the right temporal lobe. **e**, **f** The recurrent tumor at age 26. **e** Gd-T1WI shows a heterogeneously enhanced tumor in the same region. **f** A FLAIR image shows a limited edema around the tumor. Case 3 (**g**–**i**). **g** Gd-T1WI shows a homogeneously enhanced circumscribed tumor in the right frontal lobe. **h** Surrounding edema was observed in the FLAIR image. **i** Calcification was not obvious in the CT image. Case 4 (**j**–**l**). **j** Gd-T1WI shows a well demarcated mass with a homogeneous contrast enhancement within the left temporal lobe. **k** A FLAIR image shows surrounding edema. **l** No calcification was detected in the CT image

Discussion

Alternation of *ATRX* in combination with *BRAF* V600E mutation and homozygous deletion of *CDKN2A/B* is very rare in gliomas. Among 681 grade I–IV gliomas in recent reports analyzing all three genetic mutations (82 adult glioblastomas, 148 grade II and III diffuse gliomas, 368 pediatric low- and high-grade gliomas, 24 PXAs and A-PXAs, 21 PAs and PAs with anaplasia, and 40 gangliogliomas) [11–23], only one case (histologically defined as anaplastic PXA) had all three mutations [11]. Five cases (three adult glioblastomas, one grade II diffuse glioma, and one pediatric GBM) had both *BRAF* V600E mutation and *ATRX* alternation [17, 21, 22]. However, detailed histology was not reported in these studies. Moreover, we searched 2395 grade I–IV gliomas in a public database of The Cancer Genome

Table 2 Histological and immunohistochemical findings

Case	Spindle cell	Pleomorphic cell	Xanthic cell	Epithelioid cell	Piloid cell	Eosinophilic granular bodies	Necrosis	MVP	Mitosis (/10HPF)	Other findings	Initial pathological diagnosis
1	90	5	0	5	0	−	+	+	20	Accumulation of tumor cell to the subpial space and perivascular space	Glioblastoma
2	60	10	A few	5	25	−	+	−	4	Microcalcification, Hyalinization of blood vessels	Anaplastic astrocytoma
2(rec)	75	15	A few	5	5	−	+	±	6	Hyalinization of blood vessels	Localized high grade astrocytoma
3	75	5	0	20	0	±	−	−	6		Localized high grade astrocytoma
4	85	A few	0	15	0	+	−	±	8	Prominent fibrosis around blood vessels	Localized high grade astrocytoma

Case	GFAP	S-100P	Olig2	nestin	EMA	CD34	mIDH1 R132H	ATRX	BRAFV600E	p53	Ki-67 LI (%)
1	2+(s)	3+(s)	3+(s)	3+(m)	2+(m)	–	–	–	3+(w)	1+(m)	20.1
2	3+(s)	3+(s)	3+(m)	3+(s)	ND	–	ND	Sample deterioration	Sample deterioration	Sample deterioration	Sample deterioration
2(rec)	2+(s)	3+(s)	3+(m)	3+(w)	–	–	ND	–	3+(m)	2+(m)	20
3	1+(s)	2+(m)	3+(s)	3+(w)	ND	–	–	–	2+(w)	ND	13
4	3+(s)	ND	3+(s)	ND	ND	ND	–	–	3+(w)	ND	6.1

The visually estimated ratio of cellular elements (spindle, pleomorphic, xanthic, epithelioid and piloid cell) are described in percentage (%)

+ observed, ± only few observed, –not observed, /10HPF per 10 high power fields

The intensity and extent of the of immunopositive tumor cells were scored as follows: (w)—weak, (m)—moderate, (s)—strong, (−)totally negative, (1+) < 10%, (2+) 10–50%, (3+) > 50%

ND not done, *GFAP* glial fibrillary acidic protein, *S-100P* S-100 protein, *EMA* epithelial membrane antigen, *mIDH1 R132H* mutated isocirate dehydrogenase-1/2 R132Hs

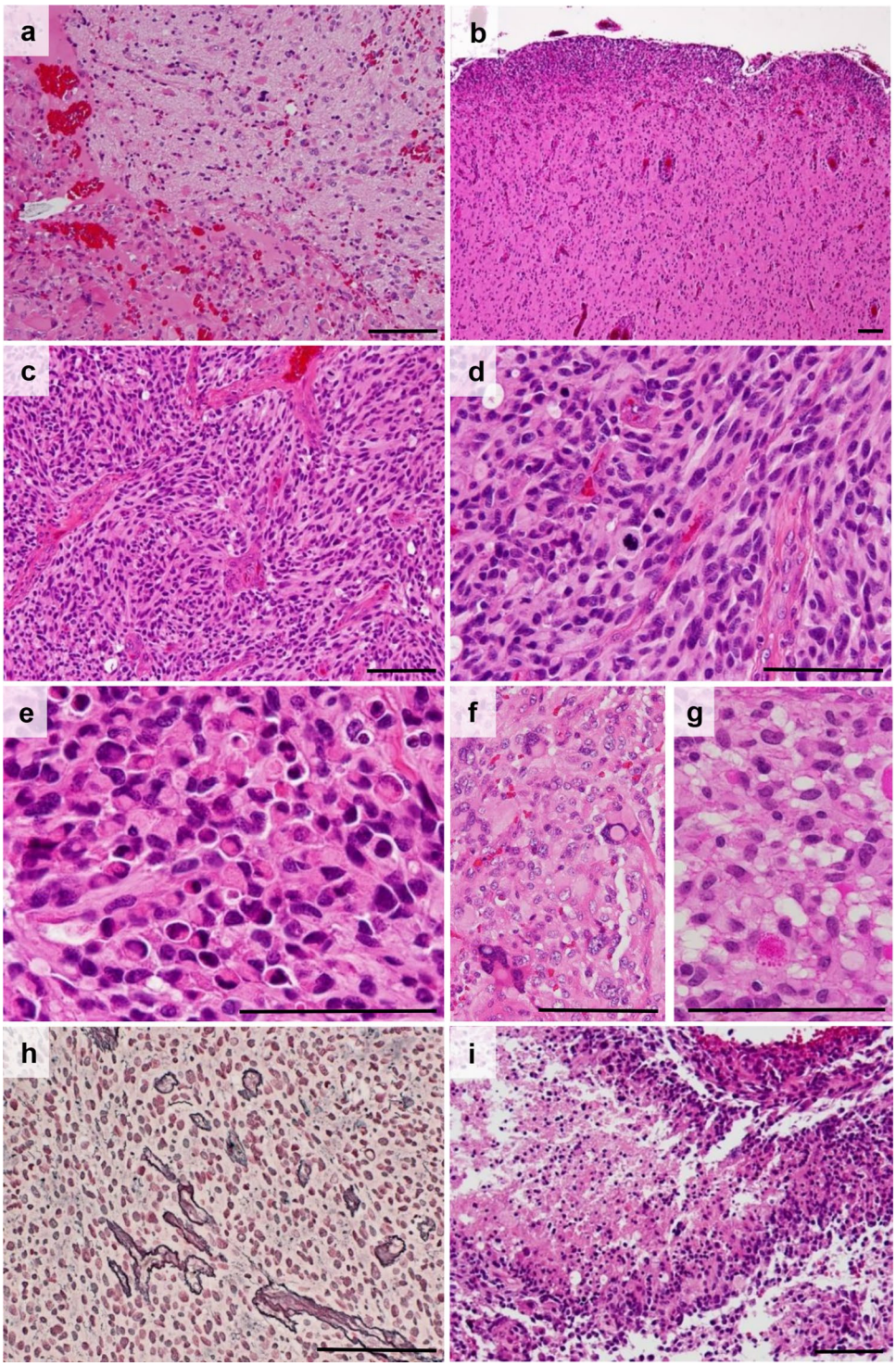

Fig. 2 Histological findings. **a** Case 2. The border between the tumor and adjacent brain parenchyma was relatively sharp. **b** Case 1. Accumulation of tumor cells in the subpial and perivascular space. **c**, **d** Case 1. Proliferation of spindle cells in a fascicular pattern with frequent mitosis is shown (arrow). **e** Case 1. Tumor cells with eccentric nuclei and round cytoplasm resembled epithelioid cells. **f** Case 3. Pleomorphic cells with bizarre nuclei. **g** Case 4. Eosinophilic granular bodies. **h** Case 1. Reticulin fibers were limited around blood vessels. **i** Case 2. Palisading necrosis. Scale bar = 50 μm (**a**–**i**)

Atlas (TCGA) (cBioPortal for Cancer Genomics: https://www.cbioportal.org), but no tumor had all three alternations.

Reinhardt et al. recently reported a subset of histologically defined anaplastic pilocytic astrocytomas, showing a common DNA methylation profile [14]. These cases had a high frequency of shared mutations in the MAPK pathway, *CDKN2A/B,* and *ATRX*. Changes in the MAPK pathway were mostly a *BRAF-KIAA1549* fusion or *NF1* mutation, and only one case had the *BRAF* V600E mutation. The case with the *BRAF* V600E mutation also had a *CDKN2A/B* alternation but no loss of ATRX immunoreactivity.

Both *BRAF* V600E mutation and *CDKN2A/B* homozygous deletion commonly occur in PXA and A-PXA.[24, 25], whereas concurrent *BRAF* V600E mutation, *CDKN2A/B*

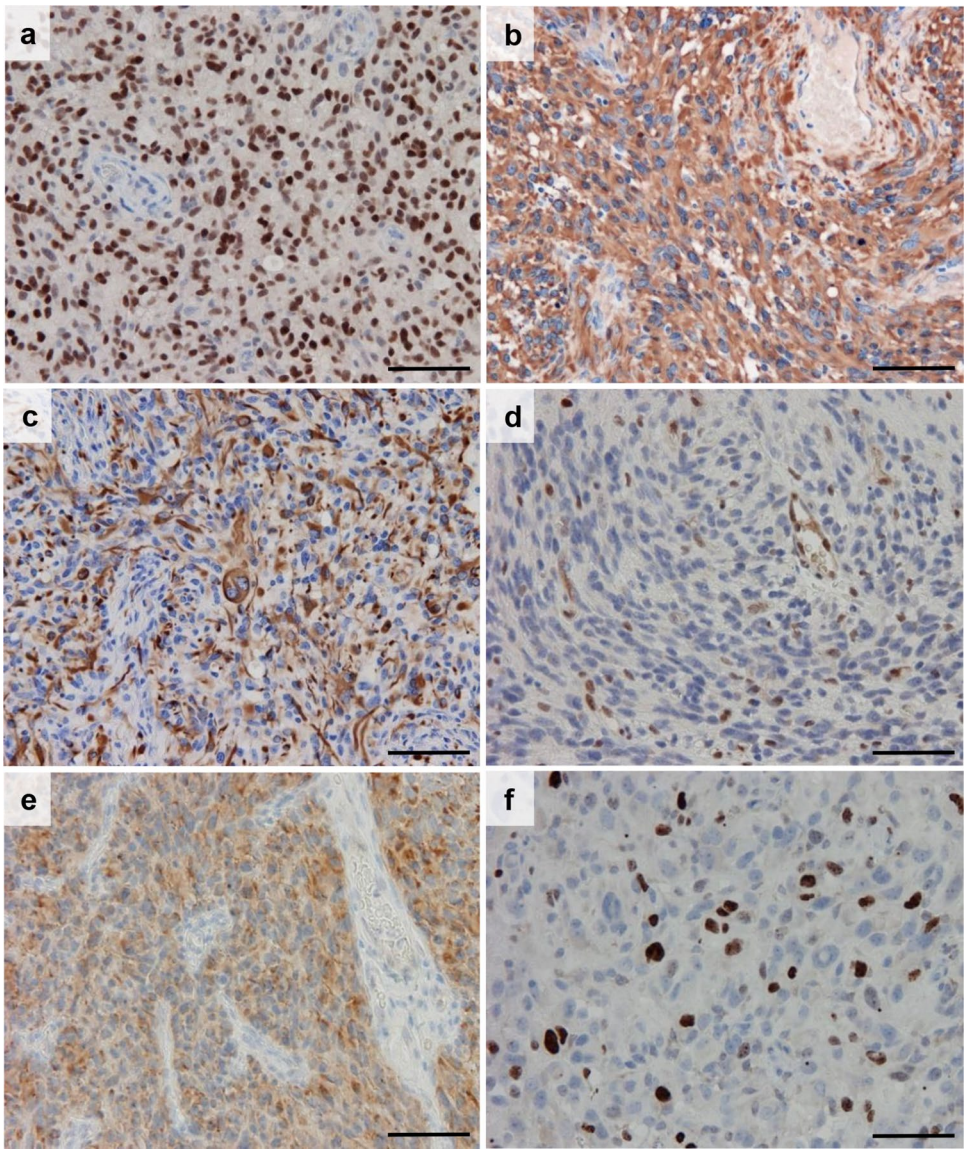

Fig. 3 Immunohistochemical findings. **a** Uninterrupted nuclear immunoreactivity for Olig2. **b** Cytoplasmic positivity for Nestin. **c** GFAP was positive in patches. **d** The tumor cell nuclei show loss of ATRX expression, but expression in vessels was retained. **e** Diffuse moderate positivity for BRAF V600E. **f** Relatively high Ki-67 labeling index is shown. **a**, **b**: case 4, **c**, **f**: case 3, **d**, **e**: case 1, Scale bar = 50 μm (**a**–**f**)

homozygous deletion, and *TERT* promoter mutation are frequent in epithelioid glioblastoma and A-PXA [10, 11]. In our current study, mutations in the *TERT* promoter were not detected, but loss of nuclear ATRX immunoreactivity was observed. This is interesting because *TERT* and *ATRX* are both telomere maintenance-related genes and are mutually exclusive in diffuse gliomas [26, 27]. Additionally, concurrent *TERT* promoter mutation, *CDKN2A/B* homozygous deletion, and *BRAF* V600E mutation are observed in a subset of melanomas and thyroid carcinomas [28, 29], but the combination of *ATRX* inactivation, *CDKN2/B* homozygous deletion, and *BRAF* V600E mutation has not been reported in other non-CNS neoplasms.

Histologically, all of our cases had a solid growth pattern, mainly composed of spindle-shaped cells with pleomorphism resembling PXA. A-PXA is sometimes misdiagnosed as glioblastoma or anaplastic astrocytoma because of its proliferative capacity [30]. In fact, tumors histologically diagnosed as A-PXA are occasionally re-classified into glioblastoma using methylation analysis [31]. The diagnosis of A-PXA can be supported not only by a demarcated border, but also numerous eosinophilic granular bodies, pleomorphic cells, and xanthic cells. In our cases, these histological features were not prominent, which made it more difficult to differentiate glioblastoma. However, all our cases resulted in an excellent post-operative state with the longest survival of 28 years. Therefore, distinguishing these tumors from glioblastoma is important from a clinical aspect.

Previous studies of gliomas harboring *BRAF* V600E reported relatively favorable prognosis compared to those without this mutation [32–35]. Chi et al. reported five low-grade diffuse gliomas with the *BRAF* V600E mutation demonstrating a distinct phenotype [36]. Several of these cases had relatively well demarcated borders. One

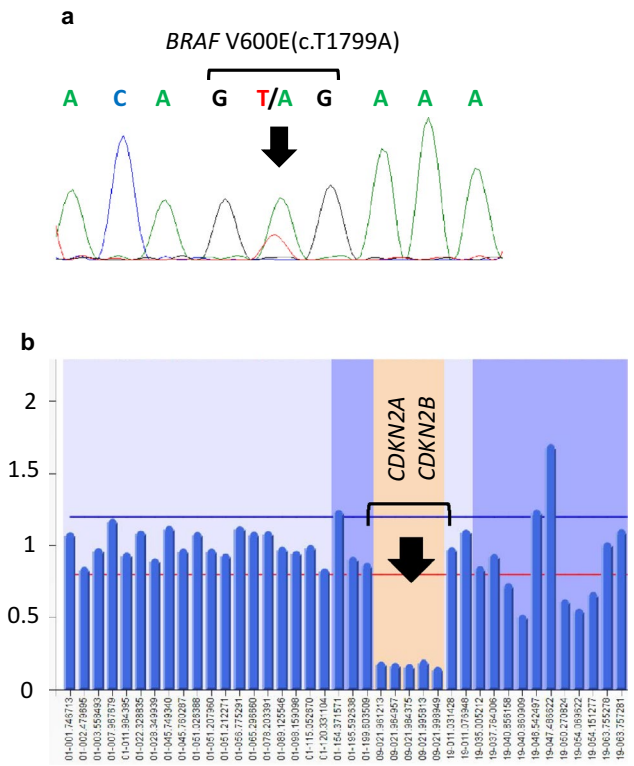

Fig. 4 Genetic findings. **a** Direct DNA sequencing of case 1. The *BRAF V600E* mutation (arrow) was detected. **b** Multiplex ligation-dependent probe amplification analysis of case 1. Homozygous deletion of *CDKN2A/B* is shown (arrow)

case had packed growth of spindle-shaped glial cells without typical characteristics of PXA, pilocytic astrocytoma, or ganglioglioma. The other case displayed proliferation of tumor cells in the subarachnoid and Virchow-Robin spaces. Although these cases were all low-grade, and the authors did not investigate mutations in *ATRX* and *CDKN2A/B*, the cases shared some clinicopathological features of our cases.

In summary, the present cases represent circumscribed high-grade astrocytomas with the unusual combination of *BRAF* V600E, *ATRX*, and *CDKN2A/B* alternations. These cases lacked typical histological characteristics of PXA and cannot be classified into the WHO classification of CNS tumors. Even with an anaplastic appearance, the prognosis was relatively favorable, and over-diagnosis of glioblastoma may be concerned. Alternations in *ATRX* and *BRAF* V600E can be readily detected by immunohistochemistry to verify the diagnosis. To understand whether these tumors are a distinct entity, or they are a subgroup of other tumors such as PXA, more cases are needed, and additional methylation analysis is worth investigating.

Acknowledgements We thank Ms. Machiko Yokota (Gunma University) for her excellent technical assistance.

Compliance with ethical standards

Conflict of interest The authors declare that they have no conflict of interest.

References

1. Giannini C, Paulus W, Louis DN, Liberski PP, Figarella-Branger D, Capper D (2016) Pleomorphic xanthoastrocytoma. In: Louis DN, Ohgaki H, Wiestler OD, Cavenee WK (eds) WHO classification of tumors of the central nervous system, 4th edn. IARC Press, Lyon, pp 94–99
2. Koelsche C, Sahm F, Capper D et al (2013) Distribution of TERT promoter mutations in pediatric and adult tumors of the nervous system. Acta Neuropathol 126:907–915
3. Korshunov A, Chavez L, Sharma T et al (2018) Epithelioid glioblastomas stratify into established diagnostic subsets upon integrated molecular analysis. Brain Pathol 28:656–662
4. Nakata S, Horiguchi K, Ishiuchi S et al (2017) A case of high-grade astrocytoma with BRAF and ATRX mutations following a long-standing course over two decades. Neuropathology 4:351–357
5. Nobusawa S, Lachuer J, Wierinckx A et al (2010) Intratumoral patterns of genomic imbalance in glioblastoma. Brain Pathol 20:936–944
6. Arai M, Nobusawa S, Ikota H, Takemura S, Nakazato Y (2012) Frequent IDH1/2 mutations in intracranial chondrosarcoma: a possible diagnostic clue for its differentiation from chordoma. Brain Tumor Pathol 29:201–206
7. Gessi M, van de Nes J, Griewank K et al (2014) Absence of TERT promoter mutations in primary melanocytic tumours of the central nervous system. Neuropathol Appl Neurobiol 40:794–797
8. Schindler G, Capper D, Meyer J et al (2011) Analysis of BRAF V600E mutation in 1,320 nervous system tumors reveals high mutation frequencies in pleomorphic xanthoastrocytoma, ganglioglioma and extra-cerebellar pilocytic astrocytoma. Acta Neuropathol 121:397–405
9. Watanabe K, Tachibana O, Sato K, Yonekawa Y, Kleihues P, Ohgaki H (1996) Overexpression of the EGF receptor and p53 mutations are mutually exclusive in the evolution of primary and secondary glioblastomas. Brain Pathol 6:217–223
10. Nakajima N, Nobusawa S, Nakata S et al (2018) BRAF V600E, TERT promoter mutations and CDKN2A/B homozygous deletions are frequent in epithelioid glioblastomas: a histological and molecular analysis focusing on intratumoral heterogeneity. Brain Pathol 28:663–673
11. Phillips JJ, Gong H, Chen K et al (2018) The genetic landscape of anaplastic pleomorphic xanthoastrocytoma. Brain Pathol 29:85–96
12. Rodriguez FJ, Brosnan-Cashman JA, Allen SJ et al (2018) Alternative lengthening of telomeres, ATRX loss and H3–K27M mutations in histologically defined pilocytic astrocytoma with anaplasia. Brain Pathol 1:126–140
13. Johnson BE, Mazor T, Hong C et al (2014) Mutational analysis reveals the origin and therapy-driven evolution of recurrent glioma. Science 343:189–194
14. Bettegowda C, Agrawal N, Jiao Y et al (2013) Exomic sequencing of four rare central nervous system tumor types. Oncotarget 4:572–583
15. Zacher A, Kaulich K, Stepanow S et al (2017) Molecular diagnostics of gliomas using next generation sequencing of a glioma-tailored gene panel. Brain Pathol 27:146–159

16. Yang RR, Aibaidula A, Wang WW et al (2018) Pediatric low-grade gliomas can be molecularly stratified for risk. Acta Neuropathol 136:641–655
17. Reinhardt A, Stichel D, Schrimpf D et al (2018) Anaplastic astrocytoma with piloid features, a novel molecular class of IDH wildtype glioma with recurrent MAPK pathway, CDKN2A/B and ATRX alterations. Acta Neuropathol 136:273–291
18. Shankar GM, Lelic N, Gill CM et al (2016) BRAF alteration status and the histone H3F3A gene K27M mutation segregate spinal cord astrocytoma histology. Acta Neuropathol 131:147–150
19. Mackay A, Burford A, Molinari V et al (2018) Molecular, pathological, radiological, and immune profiling of non-brainstem pediatric high-grade glioma from the HERBY Phase II randomized trial. Cancer Cell 33:829–842
20. Diplas BH, He X, Brosnan-Cashman JA et al (2018) The genomic landscape of TERT promoter wildtype-IDH wildtype glioblastoma. Nat Commun 9:1–11
21. Pekmezci M, Villanueva-Meyer JE, Goode B et al (2018) The genetic landscape of ganglioglioma. Acta Neuropathol Commun 6:47
22. Gielen GH, Gessi M, Buttarelli FR et al (2015) Genetic analysis of diffuse high-grade astrocytomas in infancy defines a novel molecular entity. Brain Pathol 25:409–417
23. Hong B, Banan R, Christians A et al (2018) Cerebellar glioblastoma: a clinical series with contemporary molecular analysis. Acta Neurochir (Wien) 160:2237–2248
24. Vaubel RA, Caron AA, Yamada S et al (2018) Recurrent copy number alterations in low-grade and anaplastic pleomorphic xanthoastrocytoma with and without BRAF V600E mutation. Brain Pathol 28:172–182
25. Weber RG, Hoischen A, Ehrler M et al (2006) Frequent loss of chromosome 9, homozygous CDKN2A/p14 ARF /CDKN2B deletion and low TSC1 mRNA expression in pleomorphic xanthoastrocytomas. Oncogene 26:1088–1097
26. Ceccarelli M, Barthel FP, Malta TM et al (2016) Molecular profiling reveals biologically discrete subsets and pathways of progression in diffuse glioma. Cell 164:550–563
27. Eckel-Passow JE, Lachance DH, Molinaro AM et al (2015) Glioma groups based on 1p/19q, IDH, and TERT promoter mutations in tumors. N Engl J Med 372:2499–2508
28. Hayward NK, Wilmott JS, Waddell N et al (2017) Whole-genome landscapes of major melanoma subtypes. Nature 545:175–180
29. Landa I, Pozdeyev N, Korch C et al (2019) Comprehensive genetic characterization of human thyroid cancer cell lines: a validated panel for preclinical studies. Clin Cancer Res 147371:2953
30. Yamada SM, Murakami H, Tomita Y et al (2016) Glioblastoma multiforme versus pleomorphic xanthoastrocytoma with anaplastic features in the pathological diagnosis: a case report. Diagn Pathol 11:65
31. Nakamura T, Fukuoka K, Nakano Y et al (2019) Genome-wide DNA methylation profiling shows molecular heterogeneity of anaplastic pleomorphic xanthoastrocytoma. Cancer Sci 110:828–832
32. Korshunov A, Ryzhova M, Hovestadt V et al (2015) Integrated analysis of pediatric glioblastoma reveals a subset of biologically favorable tumors with associated molecular prognostic markers. Acta Neuropathol 129:669–678
33. Zhang R, Shi Z, Chen H et al (2016) Biomarker-based prognostic stratifi cation of young adult glioblastoma. Oncotarget 7:5030–5041
34. Mistry M, Zhukova N, Merico D et al (2015) BRAF mutation and CDKN2A deletion define a clinically distinct subgroup of childhood secondary high-grade glioma. J Clin Oncol 33:1015–1022
35. Nguyen AT, Colin C, Nanni-Metellus I et al (2015) Evidence for BRAF V600E and H3F3A K27M double mutations in paediatric glial and glioneuronal tumours. Neuropathol Appl Neurobiol 41:403–408
36. Chi AS, Batchelor TT, Yang D et al (2016) BRAF V600E mutation identifies a subset of low-grade diffusely infiltrating gliomas in adults. J Clin Oncol 31:233–236